Multi-Material Decomposition Using Statistical Image Reconstruction in X-Ray CT

Yong Long and Jeffrey A. Fessler

***Abstract*—Dual-energy (DE) CT scans provide two sets of measurements at two different source energies. In principle, two materials can be accurately decomposed from DECT measurements. For triple-material decomposition, a third constraint, such as volume or mass conservation, is required to solve three sets of unknowns from two sets of measurements. An image-domain (ID) method [1] has been proposed recently to reconstruct multiple materials using DECT. This method assumes each pixel contains at most three materials out of several possible materials and decomposes a mixture pixel by pixel. We propose a penalized-likelihood (PL) method with edge-preserving regularizers for each material to reconstruct multi-material images using a similar constraint. Comparing with the image-domain method the PL method greatly reduced noise, streak and cross-talk artifacts, and achieved much smaller root-mean-square (RMS) errors.**

***Index Terms*—Computed tomography, dual energy, multi-material decomposition, statistical image reconstruction**

I. Introduction

Dual-energy (DE) CT reconstruction methods typically reconstruct images of two basis materials (*e.g.*, soft-tissue and bone) from two sets of measurements at two different X-ray source potential. However, some applications desire three or more component images [1], [2]. When quantifying the concentration of iron in a fatty liver, images of three constitute materials, iron, fat and tissue, are required [2]. For the purpose of radiotherapy, in addition to soft-tissue and bone it is also useful to know the distribution(s) of other materials, such as calcium, metal (*e.g.*, gold) and iodine.

A third criteria, such as volume conservation [1] or mass conservation [2], can enable reconstructing three basis materials from DECT measurements. Volume (mass) conservation assumes the sum of the volumes (masses) of the three constituent materials is equivalent to the volume (mass) of the mixture.

Mendonca *et al.* [1] proposed an image-domain method to reconstruct multiple materials pixel by pixel from a DECT scan. In addition to volume conservation assumption, this method assumes that each pixel contains a mixture of at most three materials and the material types can vary between pixels. It establishes a material library containing all the possible triplets of basis materials for a specific application. It obtains a dual-material-density pair through projection-based decomposition approach from DECT measurements, and then generates a linear-attenuation-coefficient (LAC) pair for each pixel at two selected distinct energies. Given a LAC pair, a material triplet and the volume conservation assumption, triple material decomposition is solvable for each pixel. This method sequentially decompose each pixel into different triplets in the material library, and collects solutions of volume fractions that satisfy a box constraint ([0 1]). If there are multiple solutions, it determines the optimal triplet as the one which has the smallest sum of distances between the original LAC pair and three LAC pairs of its constituent materials at the two selected distinct energies. If there is no feasible solution, it finds a unique multi-material decomposition by solving a mixed least-square optimization problem with volume conservation constraint.

Inspired by the image-domain method [1], we propose a penalized-likelihood (PL) method with edge-preserving regularizers for each material to reconstruct multi-material images. It is well known that statistical image reconstruction methods based on physical models of the CT system and a statistical model can obtain lower noise images. The proposed PL method considers each material image as a whole, instead of pixel by pixel, so prior knowledge, such as piecewise smoothness, can be used to help solve the reconstruction problem.

We evaluated the proposed PL method on a simulated object containing fat, blood, omnipaque300 (a common contrast agent), cortical bone and air. Comparing with the image-domain method, the PL method was able to reconstruct component images with lower noise, greatly reduce streak artifacts, and effectively alleviate the cross-talk phenomenon where a component of one material appearing in the image of another material. The RMS errors of the PL method were about 40% lower for fat, blood, omnipaque300 and cortical bone compared to the image-domain method.

The organization of this paper is as follows, Section 2 introduces the physical model and the PL method, Section 3 shows the results and Section 4 presents conclusions.

II. Method

A. Physical Models

1) Measurement Model: We use the following general model to describe the measurement physics for X-ray CT. The detector measures X-ray photon emerging from the object at $M_0 \geq 1$ different incident spectra. Let Y_{im} denote the measurement for the ray $\mathcal{L}_{im}$ which is the ith ray for the mth energy scan, where $m = 1, \ldots, M_0$, $i = 1, \ldots, N_\mathrm{d}$, and N_d is the number of rays. For a ray $\mathcal{L}_{im}$ of infinitesimal width, the mean of the projection measurements could be expressed

This work was supported in part by NIH grant HL-098686.

Y. Long and J. Fessler are with Dept. of Electrical Engineering and Computer Science, University of Michigan, Ann Arbor, MI 48109.

as:

$$\bar{y}_{im} \triangleq \int I_{im}(\mathcal{E}) \exp\left(- \int_{\mathcal{L}_{im}} \mu(\vec{x}, \mathcal{E}) \, \mathrm{d}\ell \right) \mathrm{d}\mathcal{E} + r_{im}, \quad (1)$$

where $\mu(\vec{x}, \mathcal{E})$ denotes the 3D unknown spatially- and energy-dependent attenuation distribution, $\int_{\mathcal{L}_{im}} \cdot \, \mathrm{d}\ell$ denotes the "line integral" function along line $\mathcal{L}_{im}$, the incident X-ray intensity $I_{im}(\mathcal{E})$ incorporates the source spectrum and the detector gain, and r_{im} denotes the ensemble mean of background signals. We treat each $I_{im}(\mathcal{E})$ and r_{im} as known nonnegative quantities.

2) Object Model: Assuming volume conservation [1] that volume of a mixture equals to the sum of volumes of its constituent parts, the volume fraction of the lth material at the jth pixel is $x_{lj} = V_{lj} / \sum_{l=1}^{L_0} V_{lj}$, where V_{lj} denotes the volume of the lth material at the jth pixel and L_0 denotes the number of materials of interest. We also assume that each pixel contains no more than three materials and the material types can be different among pixels. Let Θ be the triplet library containing all physically meaningful triplets formed from L_0 pre-selected materials of interest.

We describe the object model as

$$\mu(\vec{x}, \mathcal{E}) = \sum_{l=1}^{L_0} \sum_{j=1}^{N_\mathrm{p}} \mu_l(\mathcal{E}) \, b_j(\vec{x}) \, x_{lj}, \quad (2)$$

subject to

$$\begin{cases} \sum_{l=1}^{L_0} x_{lj} = 1, & \forall j, \\ \sum_{l=1}^{L_0} \mathbb{1}_{\{x_{lj} \neq 0\}} \leq 3, & \forall j \\ 0 \leq x_{lj} \leq 1, & \forall l, j \end{cases} \quad (3)$$

where $\mu_l(\mathcal{E})$ is the energy-dependent LAC of the lth material type and $b_j(\vec{x})$ denotes spatial basis functions (*e.g.*, pixels).

Let $\boldsymbol{x}$ denote the image vector $\boldsymbol{x} = (\boldsymbol{x}_1, \ldots, \boldsymbol{x}_l, \ldots, \boldsymbol{x}_{L_0}) \in \mathbb{R}^{N_\mathrm{p} \times L_0}$ for $\boldsymbol{x}_l = (x_{l1}, \ldots, x_{lj}, \ldots, x_{lN_\mathrm{p}})$ of the lth material. Combining the general measurement model (1) and the object model (2), the mean of the projection measurements $\bar{y}_{im}(\boldsymbol{x})$ is a function of $\boldsymbol{x}$. The goal of the proposed reconstruction method is to estimate $\boldsymbol{x}$ for $L_0 > 3$ subject to (3) from noisy measurements Y_{im} with $M_0 = 2$.

B. Penalized-Likelihood (PL) Reconstruction

For the case of normal clinical exposures, the X-ray CT measurements are often modeled as independently Poisson random variables with means (1), *i.e.*

$$Y_{im} \sim \mathsf{Poisson}\{\bar{y}_{im}(\boldsymbol{x})\} \, .$$

The corresponding negative log-likelihood for independent measurements Y_{im} has the form

$$- L(\boldsymbol{x}) \equiv \sum_{m=1}^{M_0} \sum_{i=1}^{N_\mathrm{d}} \bar{y}_{im}(\boldsymbol{x}) - Y_{im} \log \bar{y}_{im}(\boldsymbol{x}), \quad (4)$$

where $\equiv$ means "equal to within irrelevant constants independent of $\boldsymbol{x}$."

Component images are estimated from the noisy measurements Y_{im} by minimizing a Penalized-Likelihood (PL) cost function subject to constraints given in (3) on the elements of $\boldsymbol{x}$ as follows:

$$\hat{\boldsymbol{x}} = \underset{\boldsymbol{x} \text{ subject to } (3)}{\arg\min} \Psi(\boldsymbol{x}) \quad (5)$$

$$\Psi(\boldsymbol{x}) \triangleq -L(\boldsymbol{x}) + R(\boldsymbol{x}). \quad (6)$$

The edge-preserving regularization term $R(\boldsymbol{x})$ is

$$R(\boldsymbol{x}) = \sum_{l=1}^{L_0} \beta_l R_l(\boldsymbol{x}_l), \quad (7)$$

where the regularizer for the lth material is

$$R_l(\boldsymbol{x}_l) = \sum_{j=1}^{N_\mathrm{p}} \sum_{k \in \mathcal{N}_{lj}} \kappa_{lj} \kappa_{lk} \psi_l(x_{lj} - x_{lk}) \quad (8)$$

$$\psi_l(t) = \frac{\delta_l^2}{3} \left(\sqrt{1 + 3 \left(\frac{t}{\delta_l} \right)^2} - 1 \right), \quad (9)$$

where κ_{lj} and κ_{lk} are parameters encouraging uniform spatial resolution [3] and $\mathcal{N}_{lj}$ is some neighborhood of voxel x_{lj}. The regularization parameters β_l and δ_l can be chosen differently for different materials according to their properties.

Because the cost function $\Psi(\boldsymbol{x})$ in (6) is difficult to minimize directly, we apply optimization transfer principles to develop an algorithm that monotonically decreases $\Psi(\boldsymbol{x})$ each iteration [4]. We first find pixel-wise separable quadratic surrogates of the cost function, and then minimize them under constraints given in (3). We loop over all triplets in the pre-determined material library, minimize the surrogates under box and sum-to-one constraints in (3), and determine the optimal triplet for each pixel as the one making the surrogate of that pixel smallest. To obtain a good initialization for the iterative optimization, we use the images reconstructed by the image-domain method [1]. We use the ordered subsets approach to accelerate the "convergence" to a good local minimum [4].

III. Results

To evaluate the proposed PL method for multi-material decomposition purpose, we reconstructed volume fractions of a NCAT chest phantom [5] containing fat, blood, omnipaque300, cortical bone and air from a simulated DECT scan.

Fig. 1 shows true volume fractions and monoenergetic image at 70 keV of the simulated NCAT chest phantom. We simulated the geometry of a GE LightSpeed X-ray CT fan-beam system with an arc detector of 888 detector channels by 984 views over 360°. The size of each detector cell was 1.0239 mm. The source to detector distance was $D_\mathrm{sd} = 949.075$mm, and the source to rotation center distance was $D_\mathrm{s0} = 541$mm. We included a quarter detector offset to reduce aliasing. We used the distance-driven (DD) projector [6] to generate projections of the true object. We simulated two incident spectra of the X-ray tube voltages at 140 kVp and 80 kVp. Their corresponding effective energies were 69 keV and 47 keV. We generated noiseless measurements $\bar{y}_{im}$ of the simulated NCAT phantom using (1) and the simulated spectra. The simulated true images were 1024×1024 and the pixel size was 0.49 mm, while the reconstructed images were

512×512 and the pixel size was 0.98 mm. We introduced this model mismatch deliberately to test the multi-material decomposition methods. To the noiseless measurements $\bar{y}_{im}$, we added Poisson distributed noise corresponding to 2×10^5 incident photons per ray for rays corresponding to the 140 kVp spectrum. For the 80 kVp spectrum, we added Poisson noise corresponding to $2 \times 10^5 \cdot I_{i2}/I_{i1} = 6 \times 10^4$ incident photons per ray where I_{i1} and I_{i2} denote the total intensity of the ith ray for the 140 kVp and 80 kVp spectrum respectively.

For this simulation we let the triplet material library Θ contain seven triplets which formed from pre-selected five materials: fat, blood, omnipaque300, cortical bone and air, and which exclude the combination of omnipaque300 and cortical bone (This is based on the fact that contrast agent does not spread into the cortical bone area). We implemented the image-domain method as described in [1] to initialize the PL method. We used the conventional DE projection-based method with polynomial approximation [7] followed by FBP to reconstruct water-iodine density images and chose 70 keV and 140 keV to yield LAC pairs for the image-domain method. We also tried a more sophisticated dual-material decomposition method, the statistical sinogram restoration method proposed in [8], but the final reconstructed component images were very similar to those of using polynominal approximation. For the PL method we chose $\beta_l = 2^8, 2^{11}, 2^{11}, 2^8, 2^4$ and $\delta_l = 0.01, 0.01, 0.005, 0.01, 0.1$ for fat, blood, omnipaque300, cortical bone and air, respectively. We ran 1000 iterations of the optimization transfer algorithm with 41 subsets to accelerate the convergence. Note that (5) is a nonconvex problem so the algorithm finds a local minimum.

Fig. 2, Fig. 3, Fig. 4, Fig. 5 and Fig. 6 show estimated volume fractions of the five materials reconstructed by the PL method and the image-domain method. The grayscale values represent volume fractions of each material. The big white disks Fig. 6 were due to the elliptical reconstruction support. The streak-like artifacts in the reconstructed images by the image-domain method were very similar to those in Figure 4 in [1]. The PL method greatly reduces these streak-like artifacts. The cross-talk phenomenon is evident in the image-domain results. Fat went into the cortical bone image Fig. 5, while cortical bone presented in the blood image Fig. 3. The PL method alleviated this cross-talk phenomenon very effectively. Fig. 4 shows the horizontal profiles through the upper disk of the reconstructed omnipaque300 images on the right. The PL method corrected the positive bias introduced by the image-domain method. In addition, the PL method reconstruct component images with lower noise.

We down-sampled the simulated true component images to the sizes of the reconstructed images by linearly averaging, and then calculated the root-mean-square (RMS) error of the component fractions, $\sqrt{\frac{1}{N_{\mathrm{p}}} \sum_{j=1}^{N_{\mathrm{p}}} (\hat{x}_{lj} - x_{lj})}$ within the reconstruct support for each material based on the down-sampled images. Table I shows RMS errors of the component images reconstructed by the image-domain method and the PL method. The errors were scaled by 10^3 for easy comparison. Comparing with the image-domain method, the PL method lowered the RMS errors by about 40% for fat, blood, omnipaque300 and cortical bone.

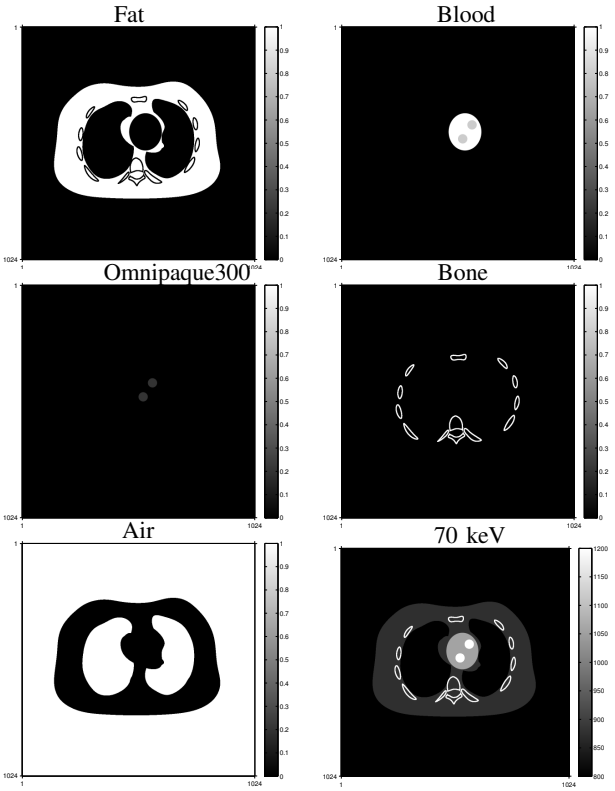

Fig. 1. True volume fractions and monoenergetic image at 70 keV.

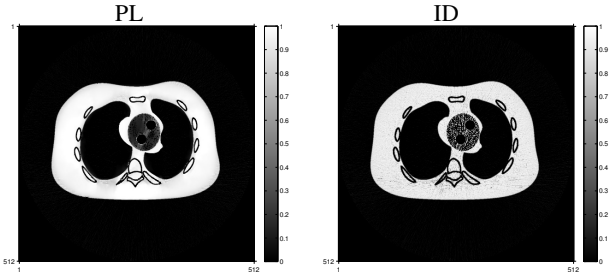

Fig. 2. Fat component results.

Method	fat	blood	omnipaque	bone	air
ID	93	73	4.4	36	46
PL	60	40	2.9	22	46

TABLE I
RMS ERROR COMPARISON OF THE RECONSTRUCTED IMAGES BY THE IMAGE-DOMAIN (ID) METHOD AND THE PL METHOD. THE ERRORS WERE UNITLESS AND ENLARGED BY 10^3.

IV. CONCLUSIONS

We proposed a statistical image reconstruction method with a PL cost function containing a negative log-likelihood term and edge-preserving regularizers for each material to decompose a mixture into multiple materials using DECT measurements. We adopted the volume conservation assumption and assumed each pixel contains no more than three materials to help solve the multi-material reconstruction problem.

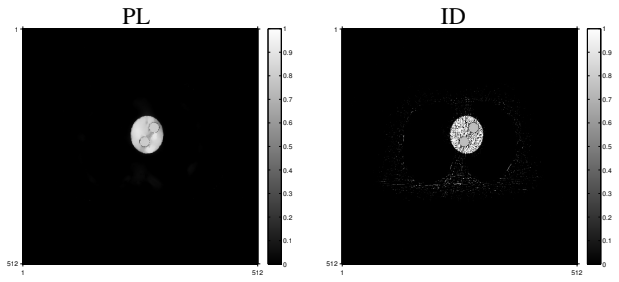

(a) Field of view (FOV) images

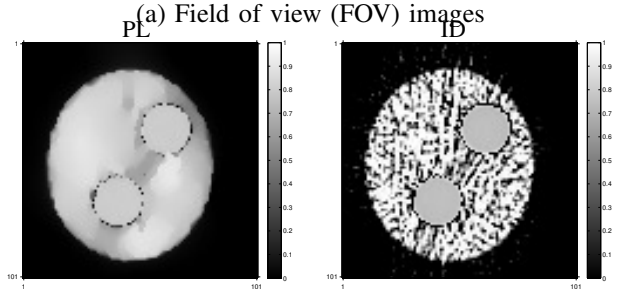

(b) Region of interest (ROI) images

Fig. 3. Bone component results.

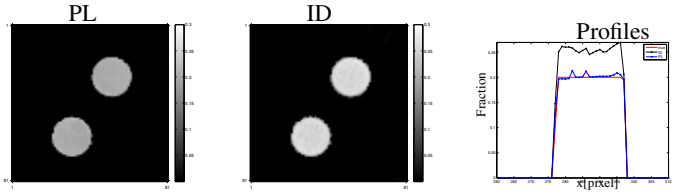

Fig. 4. Omnipaque300 component results. The right figure shows the horizontal profiles through the upper disk. The red, black and blue line denote the true, PL and ID image respectively.

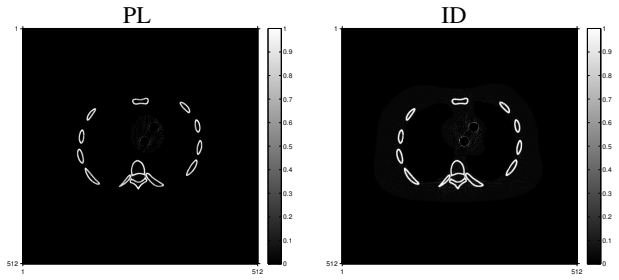

(a) Display window [0, 1]

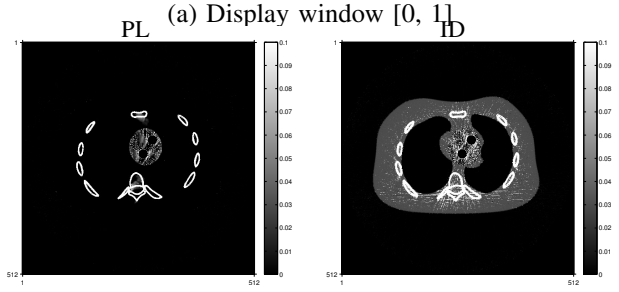

(b) Display window [0, 0.1]

Fig. 5. Cortical bone component results.

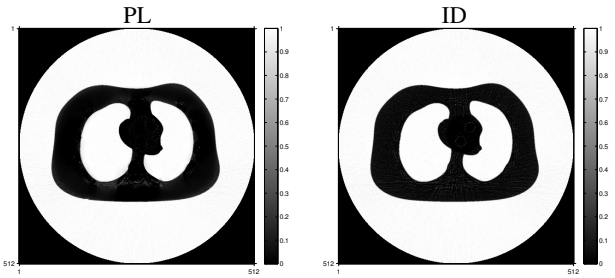

Fig. 6. Air component results.

Comparing with the image-domain method [1] that makes the same assumptions, the proposed PL method reconstructed component images with reduced noise, streak artifacts and cross-talk. The PL method was able to lower the RMS error by about 40% for fat, blood, omnipaque300 and cortical bone, compared to the image-domain method.

The PL cost function has two parameters, one regularizer coefficient β_l and one edge-preserving parameter δ_l for each material. We found that the choice of parameters for one material component influenced the reconstructed image of another component. An appropriate combination of parameters needs to be carefully determined for each application. It is also desirable for the regularizer to provide approximately uniform, isotropic and material-independent spatial resolution. Choosing regularizers for the PL method and optimizing there parameters needs further investigation.

Future work also includes applying the PL method to real data to decompose materials as many as the application needs. Since the PL cost function is non-convex, a good initialization is very important for the PL method. Future work would investigate image domain "statistica" method which is more practical than the PL method in terms of computation.

REFERENCES

[1] P. R. S. Mendonca, R. Bhotika, B. W. Thomsen, P. E. Licato, and M. C. Joshi, "Multi-material decomposition of dual-energy CT data," in *spie*, vol. 7622, 2010, p. 76221W. [Online]. Available: http://dx.doi.org/10.1117/12.844531

[2] X. Liu, L. Yu, A. N. Primak, and C. H. McCollough, "Quantitative imaging of element composition and mass fraction using dual-energy CT: Three-material decomposition," *Med. Phys.*, vol. 36, no. 5, pp. 1602–9, Apr. 2009.

[3] J. A. Fessler and W. L. Rogers, "Spatial resolution properties of penalized-likelihood image reconstruction methods: Space-invariant tomographs," *IEEE Trans. Im. Proc.*, vol. 5, no. 9, pp. 1346–58, Sep. 1996.

[4] H. Erdoğan and J. A. Fessler, "Monotonic algorithms for transmission tomography," *IEEE Trans. Med. Imag.*, vol. 18, no. 9, pp. 801–14, Sep. 1999.

[5] W. P. Segars and B. M. W. Tsui, "Study of the efficacy of respiratory gating in myocardial SPECT using the new 4-D NCAT phantom," *IEEE Trans. Nuc. Sci.*, vol. 49, no. 3, pp. 675–9, Jun. 2002.

[6] B. De Man and S. Basu, "Distance-driven projection and backprojection in three dimensions," *Phys. Med. Biol.*, vol. 49, no. 11, pp. 2463–75, Jun. 2004.

[7] R. E. Alvarez and A. Macovski, "Energy-selective reconstructions in X-ray computed tomography," *Phys. Med. Biol.*, vol. 21, no. 5, pp. 733–44, Sep. 1976.

[8] J. Noh, J. A. Fessler, and P. E. Kinahan, "Statistical sinogram restoration in dual-energy CT for PET attenuation correction," *IEEE Trans. Med. Imag.*, vol. 28, no. 11, pp. 1688–702, Nov. 2009.